ELSEVIER

Contents lists available at ScienceDirect

Applied Food Research

journal homepage: www.elsevier.com/locate/afres





Electrospun superhydrophobic polyvinyl chloride /polydimethylsiloxane-nanodiamond nanocomposite with enhanced antifouling and mechanical properties for fresh produce packaging

Shuhao Liu^a, Monica Iepure^{b,#}, Wentao Zhou^{a,#}, William DeFlorio^a, Mustafa E.S. Akbulut^{a,c}, Younjin Min^{b,d,*}

- ^a Artie McFerrin Department of Chemical Engineering, Texas A&M University, College Station, TX 77843, USA
- ^b Department of Chemical and Environmental Engineering, University of California, Riverside, CA 92521, USA
- ^c Department of Materials Science and Engineering, Texas A&M University, College Station, TX 77843, USA
- d Material Science and Engineering Program, University of California, Riverside, CA 92521, USA.

ARTICLEINFO

Keywords: Food safety Bacterial adhesion Antifouling Electrospinning Nanocomposite PFAS

ABSTRACT

Food package films serve the important functions of preserving food quality, extending shelf life, and protecting against external contaminants while also providing a barrier to moisture and oxygen. In consideration of the increasing frequency of foodborne outbreaks, there is a growing demand for food packaging films with additional functionality to prevent cross-contamination and the attachment of pathogens, thereby enhancing bacterial safety. Herein, we report a one-step fabrication approach relying on electrospinning of a blend of polyvinyl chloride (PVC) and polydimethylsiloxane (PDMS) together with nanodiamond (ND) on a rotating drum collector for the formation of bacterially antifouling food package films. In this approach, by adjusting the concentrations of PVC, PDMS, and ND and the drum angular velocity, the nanofiber diameter could be tuned in the range of 0.4 μ m to 2.0 μ m. Furthermore, these process parameters could also be used to modulate the water contact angle on the resultant films, with a minimum contact angle of 136.2 \pm 5.6° and a maximum of 159.5 \pm 3.8°. The lowest water contact angles were observed for films with bare PVC fibers while the highest contact angles were seen for films with nanocomposite fibers containing ND and PVC/PDMS. Compared with the films with bare PVC, nanocomposite films with ND-PVC/PDMS achieved up to 99.8 % and 99.6 % reduction in bacterial adhesion against *S. typhimurium* LT2 and *Listeria innocua*, respectively. The tensile strength of nanofibrous PVC film can be increased from 1.2 \pm 0.4 MPa to 4.4 \pm 0.3 MPa by the inclusion of PDMS (1:1 wt.%) and further increased to 8.9

 \pm 0.3 MPa with the additional inclusion of ND (PVC/PDMS/ND 1:1:0.1 wt.%). Considering the notable antifouling properties against bacteria and the improved mechanical characteristics, these nanocomposite films represent a noteworthy step in the development of sustainable and active food packaging solutions for a safer and healthier food supply chain.

1. Introduction

Food packaging, an essential type of food-contact surface, serves several crucial functions within the food industry (Chen et al., 2020; Khedkar & Khedkar, 2020; Konstantoglou et al., 2020; Marsh & Bugusu, 2007). First, it contains and protects food products, preventing contamination and damage during handling, storage, and distribution (Alamri et al., 2021; DeFlorio et al., 2021; Marsh & Bugusu, 2007; Vasile

& Baican, 2021). Also, proper packaging has special importance for perishable foods including meat, dairy, fruits and vegetables (Giannakourou & Tsironi, 2021; Nethra et al., 2023; Rejeesh & Anto, 2023). Second, food packaging communicates important information to consumers such as ingredients, nutrition facts, expiration dates, storage instructions, cooking directions, and additional details (Newsome et al., 2014). Third, packaging promotes food products through branding, labeling, and design (Spence, 2016). As evolution occurs in the food

E-mail address: ymin@engr.ucr.edu (Y. Min).

https://doi.org/10.1016/j.afres.2024.100417

^{*} Corresponding author.

[#] These two authors contributed equally to this work. The names are listed alphabetically.

industry, packaging has integral involvement in product development, efficient transportation of food to markets, and the provision of safety, information, and convenience to consumers.

Food-contact surfaces constitute one of the vectors contributing to bacterial contamination of food commodities (Kirchner et al., 2021; Sharma et al., 2022; Torres Dominguez et al., 2019). Pathogens can persist on conveyor belts, rollers, grading surfaces, preparation tables, and food packaging materials in food industry settings even long after exposure, serving as reservoirs for cross-contamination ((DeFlorio et al., 2021); Liu et al., 2021). For instance, Sun et al. (Sun et al., 2021) demonstrated the potential for knives to harbor and transfer bacteria, such as Escherichia coli, Salmonella, and Campylobacter, to fresh produce during food preparation. Luber et al. (Luber et al., 2006) reported the persistence of Listeria monocytogenes and the potential for cross-contamination due to inadequate sanitation and washing of cutting boards. Barbosa et al.(Barbosa et al., 2019) found Enterobacteriaceae, staphylococci and Listeria monocytogenes reusable plastic bags, indicating a risk to health due to cross-contamination. Di Ciccio et al.(Di Ciccio et al., 2020) reported that common packaging materials for cheese can harbor Listeria monocytogenes for long periods of time if stored at cool temperatures. Siroli et al. (Siroli et al., 2017) assessed the impact of fruit and vegetable packaging materials on the survival rates of various microbes during storage. Their findings revealed that under low relative humidity conditions, cardboard packaging materials promote faster declines in microbial viability compared to plastic materials, suggesting cardboard reduces the risk of food cross-contamination over storage durations. Mohammadzadeh-Vazifeh et al.(Mohammadzadeh-Vazifeh et al., 2015) reported isolation and identification of bacteria from paperboard food packaging in the range of the range of 0.2×10^3 to $>1.0 \times 10^5$ CFU/g bacterial contamination. Accordingly, beyond sustained investment in food safety regulations and training; the development of novel technologies for food-contact surfaces and packaging materials is increasingly needed to control bacterial contamination and cross-contamination across the food supply chain, tackling this significant public health problem.(DeFlorio et al., 2021)

Superhydrophobic food-contact surfaces are particularly intriguing for inhibiting bacterial attachment and biofilm formation via the manipulation of intermolecular interactions between the surface and bacteria (Li et al., 2019; Mu, Liu, et al., 2023). Specifically, superhydrophobic surfaces rely on the lotus leaf effect where micro- and nano-scale hierarchical structures create a composite interface to minimize contact area and adhesion forces (Xing et al., 2023; Xu et al., 2021). By modulating properties such as surface roughness and chemistry, the interaction forces that govern initial bacterial attachment can be altered to repel microorganisms (Encinas et al., 2020; Yang et al., 2022). Furthermore, superhydrophobic surfaces can create an extremely water-repellent layer that prevents the adhesion essential for biofilm genesis and provides a self-cleaning mechanism through the rolling motion of water droplets (Wang et al., 2021; Yilbas et al., 2021; Yu et al., 2020). However, a major fraction of superhydrophobic food-contact surfaces reported in the literature rely on fluorosilanes to coat the outermost surface and impart water super-repellency (Cremaldi & Bhushan, 2018; da Silva et al., 2023; (Mu et al., 2023); Oh et al., 2019; Zouaghi et al., 2017). Recent scientific studies have raised significant concerns about the environmental persistence and potential human toxicity of per- and polyfluoroalkyl substances (PFAS), including fluorosilanes (Dickman & Aga, 2022; Hamid et al., 2023; Holmquist et al., 2020). Potential links between PFAS and various health problems such as cancer, thyroid issues, and developmental delays have been reported in the literature (Ballesteros et al., 2017; Caron-Beaudoin et al., 2019; Oh et al., 2021; Steenland & Winquist, 2021). One of the pathways for PFAS exposure to humans involves food-contact surfaces treated with or containing PFAS compounds. For example, Schaider et al.(Schaider et al., 2017) analyzed various food packaging materials from fast food restaurants in the United States. They found that 46 % of food contact papers and 20 % of paperboard samples contained detectable fluorine,

indicating the presence of fluorinated chemicals. Notably, 33 % of samples had total fluorine levels above the detection limit, suggesting significant contamination. In essence, transitioning away from reliance on PFAS, increasingly encouraged by directives, suggestions, and regulations from regulatory bodies, is a critical contemporary research topic in the area of food safety and food-contact surfaces.

Although food packaging should be the barrier against contamination (Han et al., 2018), prior studies have revealed food can still be contaminated or cross-contaminated with packaging materials at varying extents: Patrignani et al. (Patrignani et al., 2016) reported the higher contamination level for both E.coli and Pseudomonas transferring from plastic packages to fruits compared to cardboard, while the remaining bacteria on reusable plastic bags can cause serious cross-contamination (Lo´pez-Ga´lvez et al., 2021; Patrignani et al., 2016), Recently, natural fibers have received more attention due to their abundant supply and biodegradability. Among these fibers, cellulose/lignocellulosic fibers are used for the production of composites for food packaging. However, these natural fibers have disadvantages such as lower strength and water absorption (Sydow & Bien´czak, 2019). To overcome these disadvantages, composites of cellulose and other materials have been investigated. Mohammadalinejhad et al., (Mohammadalinejhad et al., 2021) reported the composites of polylactic acid, nanosilver-doped cellulose, chitosan and lignocellulose shows the improvement in elastic modulus, tensile strength and elongation at break. However, those techniques has typically been achieved at increased production complexity with high expense and multiple steps, limiting the large-scale production for food

Electrospun nanofibers have been utilized in various industrial areas, including filtration, pharmaceuticals, food packaging, cosmetics, and protective clothing (Camerlo et al., 2013; Faccini et al., 2012; Liu et al., 2015; Tan et al., 2022; Wen et al., 2016; Zhu et al., 2019). For food packaging applications, electrospinning is an attractive technique due to its high efficiency, flexibility, and lack of requisite thermal processing. Electrospun fibers demonstrate promise for advanced structural properties, enhanced stability, and availability for multi-functionalization (Castro Coelho et al., 2021; Zhang et al., 2020; Zhao et al., 2020), These characteristics render them potentially beneficial for integration in the food production industry. Fernandez et al., (Fernandez et al., 2009) employed electrospinning to stabilize the light-sensitive compound β-carotene, an antioxidant and colorant ubiquitous in food products, via encapsulation in ultrafine zein prolamine fibers, a sustainable agropolymer. Vega-Lugo and (Vega-Lugo & Lim, 2009) prepared electrospun composites of soy protein isolate/poly(ethylene oxide) blended poly(lactic acid) for controlled release of antimicrobial agents for active food packaging applications. Moreover, recent studies support the feasibility of scaling up industrial implementations of electrospinning technology (Omer et al., 2021; Vass et al., 2020).

Herein, we report a novel type of food packaging film based on the electrospinning of a blend of polyvinyl chloride (PVC) and polydimethylsiloxane (PDMS) and nanodiamonds (ND) to form nanofibrious mesh structure with superhydrophobic characteristics. In this design, ND has been selected for several reasons. First, nanodiamonds possess remarkable mechanical properties, characterized by their exceptional hardness and wear resistance, which is attributed to their strong covalent carbon-carbon bonds (Kumar et al., 2019). Second, nanodiamonds are biocompatible and non-cytotoxic, making them well-tolerated by living organisms and suitable for various biomedical applications and drug delivery systems (Chauhan et al., 2020). Third, advancements in fabrication methods, including detonation synthesis, high-pressure high-temperature synthesis, chemical vapor deposition, and microplasma arc discharge, have contributed to the widespread commercial availability of nanodiamonds (De Feudis et al., 2020; Hammons et al., 2021; Iqbal et al., 2018). These methods have significantly reduced production costs, leading to current prices ranging from \$0.1 to \$2.0 per gram (Liu et al., 2021). Fourth, the inclusion of ND in and on electrospun fibers introduces a secondary, hierarchical texture on top of the existing

texture of fibers formed from polymeric base materials, which is necessary for achieving superhydrophobic properties. Regarding the utilization of PDMS, polysiloxanes consisting of inorganic siloxane Si-O backbones with organic methyl side groups form flexible, durable elastomeric networks that exhibit high thermal stability, biocompatibility, hydrophobicity, and oxidative resistance (Zaman et al., 2019). PDMS and organosilanes, with their inherently low surface energy, offer promising alternatives to PFAS for applications requiring low surface energy properties. Polyvinyl chloride (PVC) is the third most produced synthetic plastic, known for its versatility and wide-ranging applications in both industrial and everyday life (Facts, 2019). This polymer is valued for its durability, chemical resistance, and cost-effectiveness (Ait-Touchente et al., 2023). As such, in this study, PVC served as the primary matrix for nanocomposite fibers and the resulting film.

Scanning electron microscopy (SEM) was used for the analysis of the physical dimensions and morphological structures of the resultant nanofibers. Static water contact angle measurements and tensile testing were employed to examine the wettability and mechanical properties, respectively, of the nanofibers fabricated under different processing conditions. Bacterial repellency was studied by submerging *Salmonella typhimurium* LT2 and *Listeria innocua* cultures in contact with the materials. Furthermore, gas permeation testing was conducted to assess the transport of oxygen, carbon dioxide, and nitrogen through the inherently porous nanofibers, providing valuable insights into the potential suitability of these films for food packaging applications.

2. Material and methods

2.1. Materials

N,N-Dimethylformamide (DMF, >99.8 %) and tetrahydrofuran (THF, >99.8 %) were purchased from Thermo Scientific (Thermo Fisher Scientific Inc., Waltham, Massachusetts, USA) and used as received. Poly (vinyl chloride) (average $M_{\rm w}$ ~233,000, average $M_{\rm n}$ ~99,000) was purchased from Sigma-Aldrich (St. Louis, Missouri, USA). As the precursor of PDMS, Sylgard 184 Silicone Elastomer kit (2 part) was purchased from Dow chemistry (Midland, Michigan, USA). Nanodiamond (ND) with average size 100 nm was purchased from Henan Union Precision Material Co. Ltd. (China). Ultrapure water (resistivity of 18.2 M Ω ·cm) was collected from the ThermoFisher Barnstead GenPure ProWater Purificator (Thermo Fisher Scientific Inc., Asheville, NC, USA) and used throughout all the experiments.

For bacterial assays, tryptic soy agar (TSA), tryptic soy broth (TSB), and yeast extract were purchased from Becton, Dickinson and Co. (Franklin Lakes, NJ, USA). TSB broth was prepared at a concentration of 30 g/L, while TSA was prepared at a concentration of 40 g/L. TSB-Y broth was prepared by adding 0.6 g of yeast to 1 liter of TSB solution. After autoclaving, both TSB and TSB-Y were stored at 4 °C. TSA was used directly after autoclaving and cooling down to 44 °C without storage.

2.2. Preparation of electrospinning solutions

For comparison purposes, three different categories of nanofibers were prepared: (i) electrospun nanofibers (NF) composed of only polyvinyl chloride (NF: PVC), (ii) PVC and PDMS (NF: PVC-PDMS), and (iii) PVC, PDMS, and nanodiamond (NF: PVC-PDMS-ND). Electrospinning solutions for nanofibers composed of polyvinyl chloride (i.e., NF: PVC) were prepared by dissolving PVC powder at various concentrations (5 wt %, 7.5 wt%, and 10 wt%) in a 1:1 vol ratio mixture of dimethylformamide (DMF) and tetrahydrofuran (THF). The PVC was completely dissolved in the solvents using a magnetic stirrer for 24 h at room temperature. Electrospinning solutions for nanofibers composed of PVC and PDMS (i.e., NF: PVC-PDMS) were prepared by dissolving PVC, Sylgard A, and Sylgard B in the THF:DMF mixture at a weight ratio of 11:10:1 and rigorously stirring for 10 min. Here, the initial dissolution of PVC in the solvent mixture started 24 h ago, similar to the pure PVC

case. Electrospinning solutions for NF: PVC-PDMS-ND were very similar to that of NF: PVC-PDMS with the exception that additional nanodiamond was introduced into the solution with a PVC to ND weight ratio of 10:1. In this case, the final weight ratios of PVC, PDMS (Sylgard A+B), and ND were 10:10:1. All polymer solutions were used immediately after preparation.

2.3. Fabrication of nanofibers

An electrospinning system consisting of a programmable syringe pump (New ERA pump systems Inc., Farmingdale, NY, USA), a highvoltage power supply (Wys-30-1, China), and an electrospinning rotary drum collector (Wys-074, China) was employed for the fabrication of nanofibers. The entire setup was placed on a rubber mat and enclosed within an acrylic glass box to ensure constant environmental conditions (Wen et al., 2019). The distance between the needle tip and the collector was set to 15 cm, and the collector drum was covered with aluminum foil for efficient sample collection. Three different rotating speeds (500 rpm, 1000 rpm, and 2000 rpm) were utilized for each polymer solution. A high voltage of 25 kV was applied to the metal needle, while the collector remained grounded. Polymer solutions were loaded into syringes and injected at a constant flow rate of 1.5 mL/hr for 6 h. The resulting nanofibers were categorized based on their composition and processing conditions, adhering to a standardized naming convention that incorporates PVC concentration, PDMS presence (if applicable), ND presence (if applicable), and rotating speed. Fig. 1 provides a complete overview of all combinations of the 27 fabricated nanofibers, including their labels and corresponding fabrication parameters.

2.4. Morphological characterization of the nanofibers

The morphological structure of the nanofibers was characterized using an ultra-high-resolution field emission scanning electron microscope (FE-SEM, JSM-7500F, JEOL Ltd., Tokyo). To ensure surface electrical conductivity for accurate imaging, the nanofibers were coated with 10 nm of palladium/platinum prior to FE-SEM analysis using a sputter coater (208HR, Cressington Scientific Instruments, Watford, UK). The average fiber diameters were subsequently analyzed using Gwyddion software (Czech Metrology Institute, Brno, Czech Republic). For each sample, five different SEM micrographs were analyzed where all nanofibers were selected from the topmost layer to ensure the accuracy of the results. To further investigate the internal structure of the nanofibers and the distribution of ND, particularly in samples containing ND, cross-sectional SEM images were also acquired from samples frozen in liquid nitrogen and subsequently fractured.

2.5. Investigation of wetting behavior

The wettability of the nanofibers was evaluated by measuring the static water contact angle using the sessile drop technique. A constant volume (5 $\mu L)$ of ultrapure water was deposited on the surface of each fiber. The image of the water droplet was captured and analyzed using ImageJ software (National Institutes of Health, Bethesda, MD, USA) equipped with the Low-Bond Axisymmetric Drop Shape Analysis (LBADSA) plugin to determine the static water contact angle. The reported contact angle values represent the average of three measurements obtained from separate samples at room temperature.

2.6. Mechanical strength of the nanofibers

The mechanical properties of the nanofibers were characterized by tensile testing using a universal testing system (Next Generation 6800, Instron, Norwood, MA, USA) equipped with a 500 N force sensor. Prior to testing, the nanofibers were carefully cut into rectangular strips with dimensions of 1 cm by 5 cm. The fibers were then peeled off the aluminum surface with minimal force and secured in the clamps of the

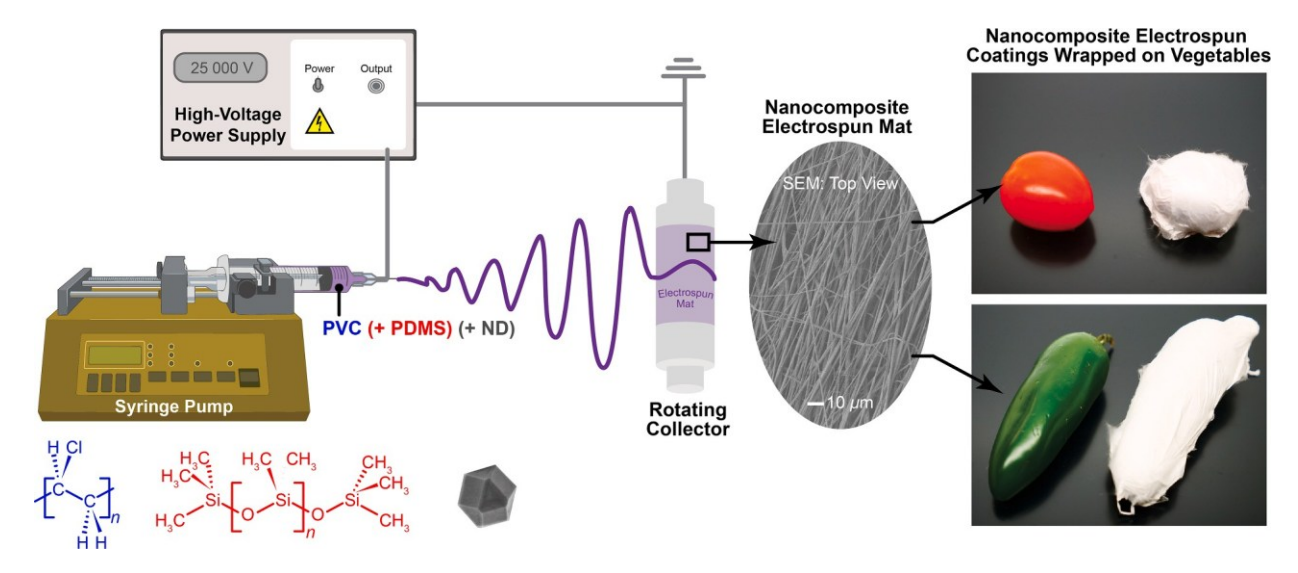


Fig. 1. Schematic illustration of the electrospinning process and its potential applications in food packaging technology.

testing system, ensuring a 3 cm gauge length of the rectangular sample was exposed for testing.

Tensile tests were performed at a constant strain rate of 1 mm/min until the force reached 90 % of the peak force, thereby capturing the full stress-strain behavior of the material. The Bluehill software from Instron was used to control the entire experiment and analyze the acquired data.

2.7. Bacterial assays

The interactions between bacterial suspension and film made from nanofibers were evaluated using a plate counting assay with two bacterial strains: Gram-positive Listeria innocua (NADC 2841) and Gramnegative Salmonella enterica serovar typhimurium LT2 (ATCC 700720). Bacterial cultures were prepared following established protocols in the literature (Arcot et al., 2023; Hashemi et al., 2022; Zhang et al., 2015, 2014). Briefly, a loopful of each strain was transferred from a tryptic soy agar (TSA) slant to separate 15 ml Falcon tubes containing 9 ml of tryptic soy broth (TSB) or tryptic soy broth supplemented with yeast extract (TSB-YE) for Listeria and Salmonella, respectively. The tubes were then incubated at 37 °C for 24 h. Subsequently, a loopful of each bacterial suspension was transferred to fresh 9 ml TSB or TSB-YE and incubated again for 24 h under the same conditions. The bacterial suspensions were then centrifuged at 4000 rpm for 10 min, and the supernatant was discarded. The bacterial pellets were resuspended in 0.1 % peptone water and washed three times by centrifugation and resuspension to remove residual media. The final bacterial suspensions in peptone water had population densities ranging from 8.8 to 9.2 log₁₀ CFU/ml and were used for subsequent experiments.

To evaluate the antifouling properties, the films made from nanofibers were cut into 1 cm × 1 cm squares and adhered to the bottom of sterilized petri dishes with the film surface facing upwards. The bacterial suspension was then gently poured onto the film samples, ensuring complete immersion. To minimize evaporative loss, the plates were sealed. Following incubation for 24 h at room temperature, the nanofiber squares were carefully peeled off the aluminum foil and rinsed three times with sterile ultrapure water using a dipping technique to remove non-adherent bacteria. The remaining bacteria, unremoved by rinsing, were quantified by the pour plate method. Then, the film squares were transferred to 9 ml of peptone water after rinsing and subjected to vortexing for 3 min to detach any adherent bacteria. The bacterial suspension was then serially diluted 10-fold several times in fresh peptone water. Next, 1 ml aliquots from each dilution were spread onto separate petri dishes and uniformly mixed with cooled tryptic soy agar (TSA) at 44 °C. After incubation for 24 h at 37 °C, the colonyforming units (CFUs) on each TSA plate were counted, allowing determination of the bacterial population density. To ensure accuracy, the experiment was repeated three times, and the results were averaged.

2.8. Gas permeation and water evaporation test

The gas permeation properties of the nanofibers were evaluated using two different gases: carbon dioxide (CO₂) and oxygen (O₂). Each film sample was secured in a 25 mm diameter stainless steel filter holder (Sigma-Aldrich, St. Louis, Missouri, USA). A digital dry pressure gauge was connected upstream of the filter holder to measure the gas pressure before it passed through the nanofibers. A bubble flow meter with a 100 mL volume scale filled with soap water was placed downstream of the filter holder. Videos of the bubble flow meter were recorded with a digital camera (H-HAS12035, Panasonic, Japan) during gas flow. Each sample was tested at a minimum of three different pressures ranging from 0 to 1 psi. The volumetric flow rate of the gas was determined by analyzing the passed volume and time through the recorded videos. Subsequently, the gas permeability of the nanofibers was calculated using the following equation:

$$\kappa = \frac{V/t}{A \times (P - P_2)} \tag{1}$$

Here, κ is the gas permeability, V is the measured volume (mL) of gas bubble passed, t is the time (s) for the bubble to move across the film, A is the effective area of the film (cm²), and ΔP is the pressure drop represented by P_1 - P_2 (Asghari et al., 2018). In this experimental setup, P_1 is the gauge pressure (atm) applied, which was read from the pressure gauge, and P_2 is atmospheric pressure, which was regarded as 0 atm in the calculation.

3. Results and discussion

3.1. Dependence of nanofiber diameter on electrospinning solution parameters

The performance and functionality of films comprised of electrospun nanofibers depend not only on the intrinsic characteristics of the individual fibers themselves but also greatly on their collective assembly and organizational alignment within the cohesive film (Zhang et al., 2023). For example, the pore size distribution arising from interfibril spaces profoundly influences vapor diffusion, fluid permeation, and cellular migration (J. Lee et al., 2022; Zhang et al., 2023). Meanwhile, overall porosity and tortuosity factors derived from nano- to micro-scale fiber

packing density and network interconnectivity modulate mechanical rigidity and bulk transport phenomena (Chavoshnejad & Razavi, 2020). As a first step of this collective analysis, we first characterized the morphological details of each fiber as a function of electrospinning solution parameters, such as concentration of PVC, PDMS, and ND and drum rotation speed. Fig. 2 compares SEM micrographs of NF: PVC, NF: PVC-PDMS, and NF: PVC-PDMS-ND. The surfaces of the pure PVC fibers were observed to be relatively smooth and uniform (Fig. 2a). The nanofibers containing both PVC and PDMS displayed more wavy/undulated surfaces and distinct boundaries compared to the bare PVC surfaces, since the interfacial affinity between the two compounds is not fully miscible (Fig. 2b). After introducing nanodiamond into the electrospinning polymer solution, large amounts of nanoscale protrusions were evident on the surfaces of each resulting nanofiber. The red arrows in Fig. 2c indicate these small hills exhibiting diameters of ~100 nm, which were exclusively observed in NF: PVC-PDMS-ND. Therefore, we can infer that the increased surface roughness of the NF: PVC-PDMS-ND is caused by protrusion of the ND particles.

Table 1 summarizes the variation in fiber diameter as a function of all electrospinning parameters: drum rotation speed and concentration of PVC, PDMS, and ND. The findings reveal that for all three electrospinning solutions (NF: PVC, NF: PVC-PDMS, and NF: PVC-PDMS-ND), fiber diameter did not significantly change with increasing drum rotation speed. However, increasing concentration consistently led to an increase in diameter for all cases. Doubling the concentration of PVC in NF: PVC resulted in a two-fold increase in the fiber diameter. In contrast, doubling the combined concentration of PVC and PDMS in NF: PVC-PDMS led to a four-fold increase in diameter, suggesting a synergistic effect between the two polymers. For NF: PVC-PDMS-ND, doubling the combined component concentration resulted in a three-fold increase in diameter, falling between the responses of the other two solutions. Notably, compared to pure PVC nanofibers, the addition of PDMS and ND did not significantly alter the fiber dimensions. This could be attributed to the fact that PDMS exhibits high elasticity (Huang et al., 2021), which might allow it to deform and adapt to the stretching forces during electrospinning without substantially impacting the overall fiber diameter. Furthermore, the weak intermolecular interactions at the interface between PDMS and PVC phases (Xu et al., 2010) might also contribute to these observed trends. Our further investigations focused on understanding the effect of rotation speed on the inter-fiber spacing, fiber alignment, and organization. To this end, we varied the drum rotation speed from 500 rpm to 1000 rpm to 2000 rpm for NF: PVC-PDMS-ND. The micrographs for samples NF: PVC-PDMS-ND [10 wt%, 500 rpm], NF: PVC-PDMS-ND [10 wt%, 1000 rpm], and NF: PVC-PDMS-ND [10 wt%, 2000 rpm] are shown in Fig. 3. Increasing the rotating speed resulted in the formation of more densely packed and oriented nanofibers. At higher rotation speeds, enhanced directional stretching arises from greater tangential mechanical forces exerted on the extruded polymer jet. This effect can orient polymer chain segments along the spinning axis, reducing fiber diameters while also facilitating tighter interfibrillar packing (Rashid

Table 1

Average diameters of electrospun nanofibers prepared under different conditions.

Sample	Concentration	500 rpm	1000 rpm	2000 rpm
PVC	5.0 wt%	0.47 ± 0.11	0.54 ± 0.17	0.46 ± 0.09
		μm	μm	μ m
	7.5 wt%	0.69 ± 0.24	0.61 ± 0.21	0.66 ± 0.32
		μm	μm	μm
	10.0 wt%	0.98 ± 0.16	1.15 ± 0.54	1.06 ± 0.56
		μm	μm	μm
PVC-PDMS	5.0 wt%	0.42 ± 0.15	0.51 ± 0.23	0.43 ± 0.10
		μm	μm	μm
	7.5 wt%	0.96 ± 0.38	0.98 ± 0.27	0.91 ± 0.26
		μ m	μ m	μm
	10.0 wt%	1.63 ± 0.67	1.35 ± 0.45	1.96 ± 1.04
		μm	μm	μm
PVC-PDMS-ND	5.0 wt%	0.42 ± 0.14	0.49 ± 0.17	0.57 ± 0.18
		μm	μm	μm
	7.5 wt%	0.95 ± 0.36	0.90 ± 0.33	0.97 ± 0.37
		μ m	μ m	μ m
	10.0 wt%	1.10 ± 0.53	1.25 ± 0.65	1.25 ± 0.67
		μm	μm	μm

et al., 2021; Xue et al., 2019). Consequently, we observed the formation of more densely arranged and aligned nanofiber bundles with increasing drum rpm. Analyses of functional performance, including diffusion barrier characteristics, wetting dynamics, and mechanical strength will provide insights into the significance of these nanostructural details and their potential impact on the material's overall properties.

3.2. Water contact angles of electrospun thin films

The wetting behavior of a liquid on a solid surface, quantified through the contact angle, is governed by an interplay of chemical and topographical factors at the solid-liquid interface (Lo "ßlein et al., 2022; Sun et al., 2022). The water contact angle (WCA) is a key parameter that quantifies the wettability of a surface, indicating its affinity for water. To determine the relative affinity of water towards the developed thin films, we measured the static WCA for all conditions. Fig. 4 shows that the static WCA of thin films based on NF: PVC [10 wt%, 2000 rpm], NF: PVC-PDMS [10 wt%, 2000 rpm], and NF: PVC-PDMS-ND [10 wt%, 2000 rpm] are $141^{\circ} \pm 6^{\circ}$, $150^{\circ} \pm 6^{\circ}$ and $159^{\circ} \pm 4^{\circ}$, respectively. Given that a flat, smooth PVC surface demonstrates a WCA of 80°-85° (Erbil, 1994), the observed WCA of ~140° in surfaces made from fibrillar PVC highlights the significance of surface texture. Blending PVC with PDMS and nanodiamond additives introduced chemical and nanotextural modulations, respectively, capable of adjusting the WCA. PDMS exhibits low surface energy due to its hydrophobic dimethyl groups (Lamberti et al., 2012). Meanwhile, the protrusion of faceted 100 nm diamonds created hierarchical surface roughness. Specifically, while the presence of PDMS can account for lowering of effective surface energy of the resultant materials, the presence of ND facilitates the formation of hierarchical textures that are characteristic of superhydrophobic surfaces.

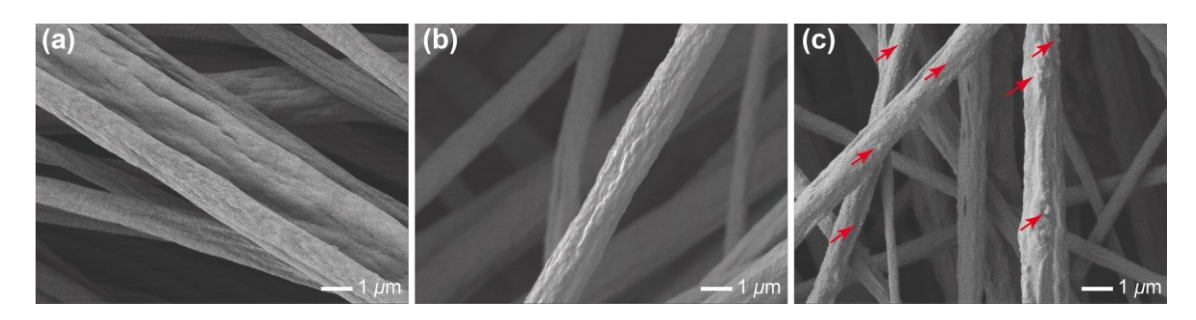


Fig. 2. SEM images of the nanofibers with different compositions and preparation conditions: (a) NF: PVC [10 wt%, 2000 rpm], (b) NF: PVC-PDMS [10 wt%, 2000 rpm], and (c) NF: PVC-PDMS-ND [10 wt%, 2000 rpm]. The red arrows in (c) indicate ~100 nm nanodiamonds on the nanofiber surfaces.

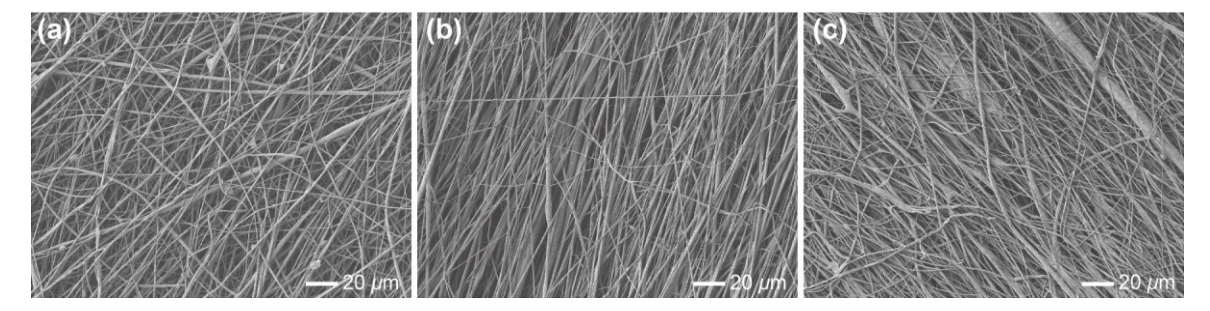


Fig. 3. SEM images of nanofibers containing PVC, PDMS, and ND prepared at different drum collector rotation speeds: (a) NF: PVC-PDMS-ND [10 wt%, 500 rpm], (b) NF: PVC-PDMS-ND [10 wt%, 1000 rpm], and (c) NF: PVC-PDMS-ND [10 wt%, 2000 rpm].

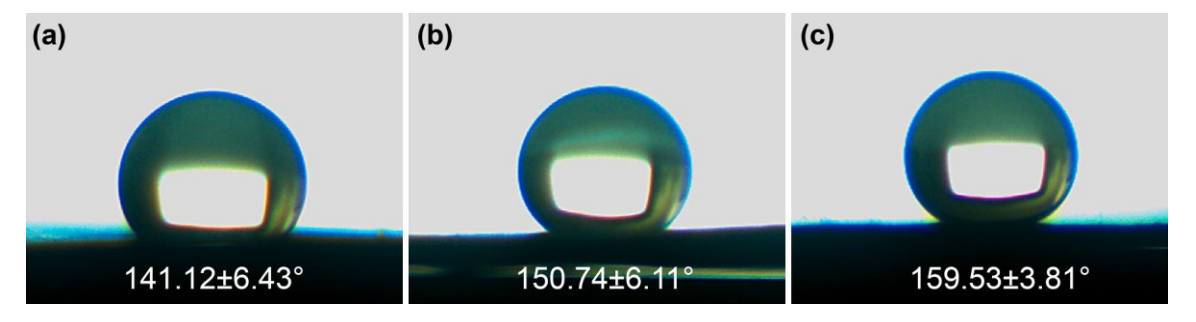


Fig. 4. Static water contact angle of thin films prepared from electrospinning solutions of (a) NF: PVC [10 wt%, 2000 rpm], (b) NF: PVC-PDMS [10 wt%, 2000 rpm], and (c) NF: PVC-PDMS-ND [10 wt%, 2000 rpm]. The values represent the mean ± standard deviation of at least three measurements.

As surface roughness increases, the wetting response can shift from Wenzel homogeneous wetting to Cassie-Baxter heterogeneous wetting, containing air pockets underneath the droplets (Bormashenko, 2019). Trapped air implies the formation of a composite solid-liquid and liquid-air interface that reduces the overall droplet contact area, facilitating beading and allowing droplets to easily roll off surfaces as roughness furtherincreases (Zhang et al., 2021).

Table 2 presents water contact angle (WCA) data for electrospun nanofibers of PVC, PVC-PDMS, and PVC-PDMS-ND at different concentrations and drum rotation speeds. Overall, all samples exhibit high contact angles (136° - 159°), indicating either very hydrophobic or superhydrophobic behavior. This is likely due to the combined effect of the internal nanostructures produced by electrospinning and the inherent hydrophobic properties of PDMS. The addition of PDMS and ND generally increased the contact angles compared to pure PVC. This

Table 2Static water contact angle of electrospun thin films prepared under different conditions.

Sample	Concentration	500 rpm	1000 rpm	2000 rpm
PVC	5.0 wt%	139.31 ± 2.96°	139.18 ± 6.31°	136.20 ± 5.58°
	7.5 wt%	138.77 ± 3.65°	143.36 ± 3.99°	141.24 ± 6.43°
	10.0 wt%	137.22 ± 5.13°	142.32 ± 3.84°	139.39 ± 3.04°
PVC-PDMS	5.0 wt%	142.42 ± 4.55°	148.70 ± 3.99°	148.98 ± 6.59°
	7.5 wt%	143.30 ± 6.53°	150.74 ± 2.84°	150.96 ± 6.11°
	10.0 wt%	152.79 ± 3.61°	152.38 ± 2.33°	153.32 ± 1.94°
PVC-PDMS-ND	5.0 wt%	154.28 ± 4.16°	155.93 ± 3.31°	155.99 ± 2.83°
	7.5 wt%	156.19 ± 2.52°	159.35 ± 5.61°	159.54 ± 3.81°
	10.0 wt%	157.31 ± 2.66°	159.30 ± 5.44°	158.19 ± 3.57°

suggests that these components contribute to the surface roughness or introduce additional hydrophobic functionalities, enhancing water droplet repulsion. Increasing the concentration slightly increased the contact angle for all samples. This could be attributed to the formation of thicker fibers or larger pores at higher concentrations, potentially trapping more air and hindering water droplet spread. Within the tested range, the effect of drum rotation speed had minimal influence on the surface roughness or air entrapment properties of the nanofibers.

3.3. Tensile strength of electrospun thin films

Tensile strength represents the maximum stress a material can withstand while being stretched or pulled before mechanical failure (Mohsin et al., 2020). It is an important mechanical performance metric for assessing durability and robustness. For food packaging applications, sufficient tensile strength is necessary for maintaining integrity during production, handling, transportation, and usage to reliably contain products (Bangar et al., 2021). For example, polymeric packaging films experience tension while being conveyed rapidly across rollers during manufacturing into bags, wraps or pouches (Rammak et al., 2021). Once formed, packages require adequate strength to avoid splits, punctures or leaks under loads inside boxes being shipped long distances (Costa et al., 2021). Finally, consumers frequently manipulate packaging - bags experiences stress during opening, microwaveable pouches swell under heating, and wrappers endure abrasion in pockets or purses (Arora & Padua, 2010). Packaging with high tensile strength provides a better barrier against external pressures and environmental factors such as moisture and air. Accordingly, we have also investigated the tensile strength of the developed electrospun films. The summary of our key findings is presented in Table 3. The tensile strength values vary significantly across the samples, ranging from 0.68 MPa to 8.86 MPa. This indicates that the composition and processing parameters have a substantial impact on the mechanical properties of the nanofibers.

For pure PVC, the tensile strength generally increases with concentration at 1000 rpm and 2000 rpm, reaching a maximum at 10 wt%. However, at 500 rpm, the trend is less clear, suggesting that the effect of

Table 3Tensile strength of electrospun thin films prepared under different conditions.

Sample	Concentration	500 rpm	1000 rpm	2000 rpm
PVC	5.0 wt%	1.52 ± 0.23	2.42 ± 0.28	1.22 ± 0.36
		MPa	MPa	MPa
	7.5 wt%	0.77 ± 0.24	1.53 ± 0.25	5.06 ± 0.99
		MPa	MPa	MPa
	10.0 wt%	1.53 ± 0.03	4.63 ± 0.57	4.71 ± 0.29
		MPa	MPa	MPa
PVC-PDMS	5.0 wt%	6.33 ± 0.91	4.47 ± 0.44	4.41 ± 1.21
		MPa	MPa	MPa
	7.5 wt%	0.68 ± 0.36	1.06 ± 0.48	3.22 ± 0.18
		MPa	MPa	MPa
	10.0 wt%	1.91 ± 0.19	3.08 ± 0.38	2.38 ± 0.62
		MPa	MPa	MPa
PVC-PDMS-ND	5.0 wt%	3.36 ± 0.39	3.04 ± 0.40	8.86 ± 2.25
		MPa	MPa	MPa
	7.5 wt%	1.28 ± 0.48	1.56 ± 0.66	2.63 ± 1.04
		MPa	MPa	MPa
	10.0 wt%	0.98 ± 0.08	1.48 ± 0.36	2.35 ± 0.24
		MPa	MPa	MPa

concentration on tensile strength might be more pronounced at higher drum collector speeds. In PVC-PDMS and PVC-PDMS-ND composites, the relationship is not straightforward, indicating that the addition of PDMS and ND alters the way concentration affects tensile strength. This behavior may be attributed to the fact that high PVC concentrations allow greater chain overlap and entanglements in the pure polymer, which bolster matrix connectivity (Hong & Chen, 1999; Shenoy et al., 2005; Wool, 1993). However, when adding PDMS and ND components, the second phases can disrupt PVC network formation and ease of chain movements at interfaces. The addition of PDMS and ND to the PVC matrix introduces new interfaces and interactions within the composite material. PDMS, being a flexible and non-polar polymer, might interfere with the alignment and packing of PVC chains, especially under varied stirring conditions. The incorporation of ND particles introduces additional variables, such as particle dispersion and particle-matrix adhesion (Lebar et al., 2021; Yuan et al., 2021). The complex interplay between these factors, including the concentration, drum collector speeds, and the presence of secondary phases, can lead to non-linear trends in tensile strength, collectively governing their mechanical behaviors.

Across all samples, the drum rotation speed shows varied impact. For pure PVC, the tensile strength peaks at 1000 rpm for higher concentrations (7.5 wt% and 10 wt%), but decreases at 2000 rpm. This may suggest optimal alignment or distribution of polymer chains at 1000 rpm. In contrast, for PVC-PDMS and PVC-PDMS-ND composites, the highest tensile strengths are generally not observed at the intermediate the rotation speeds, indicating different interaction dynamics in the presence of PDMS and ND. The PVC-PDMS composite generally exhibits higher tensile strength at 5 wt% concentration compared to PVC and PVC-PDMS-ND, especially at 500 rpm and 1000 rpm. This could be attributed to the reinforcing effect of PDMS at this concentration. However, at higher concentrations, this advantage diminishes.

The addition of ND to the PVC-PDMS composite leads to a substantial increase in tensile strength at 2000 rpm for the 5 wt% concentration, potentially due to the reinforcing effect of the ND particles. The addition of PDMS and ND significantly alters the tensile strength profile of the PVC fiber-matrix. The PVC-PDMS blend generally exhibits increased tensile strength at lower concentrations and lower drum collector speeds, while the inclusion of ND further enhances this effect, particularly at higher drum collector speeds. In conclusion, the tensile strength of PVC-based nanofibers is significantly influenced by factors such as concentration, drum collector rotation speed, and the addition of PDMS and ND, with the largest tensile strength was being observed for NF: PVC-PDMS-ND [5 wt%, 2000 rpm].

To gain more insights into the aforementioned tensile strength trends, we carried out cross-sectional scanning electron microscopy (SEM) analysis of mechanically fractured thin films. Fig. 5 displays resulting micrographs for electrospun samples NF: PVC [10 wt%, 2000 rpm], NF: PVC-PDMS [10 wt%, 1000 rpm], and NF: PVC-PDMS-ND [10 wt%, 2000 rpm]. As a baseline reference, the PVC sample showcases a remarkably uniform single-phase cross-sectional surface, devoid of any voids or defects. This signifies a well-organized and structurally sound fiber morphology. In contrast, the introduction of PDMS at this specific concentration and drum collector rotation speed results in the emergence of apparent pores and cracks within the fibers. This observation suggests a potential interfacial energy mismatch between the hydrophobic PDMS and the PVC matrix, leading to structural imperfections. The SEM analysis further reveals the intriguing distribution of ND particles within the composite fibers. They are not merely confined to the fiber surface but also embedded within, indicating their intimate integration into the PVC-PDMS matrix. This underscores the ability of ND to not only influence the bulk mechanical properties of the fibers but also actively modulate their surface morphology and potentially alter their surface interactions. The observed morphological changes in the PVC-PDMS-ND composites, particularly the presence of pores and cracks, can offer a plausible explanation for their lower tensile strength compared to pure PVC at certain concentrations and drum collector rotation speeds. These imperfections act as stress concentrators, weakening the overall structure and compromising its ability to withstand tensile forces. However, the presence of ND, despite its potential drawbacks in terms of interfacial compatibility with the PVC-PDMS matrix, might also contribute to enhanced strength through other mechanisms, such as reinforcing the polymer matrix or altering its crystallization behavior. Further investigations are necessary to fully elucidate the complex interplay between ND, PDMS, and the overall mechanical properties of the composite fibers.

3.4. Quantification of bacterial attachment to electrospun thin films

After confirming the hydrophobicity and superhydrophobicity of nanofibers, we measured the bacterial repelling behavior of these fibers by using gram-negative *S. typhimurium* LT2 and gram-positive L. *innocua* as testing cultures. Table 4 summarizes the attachment behavior of

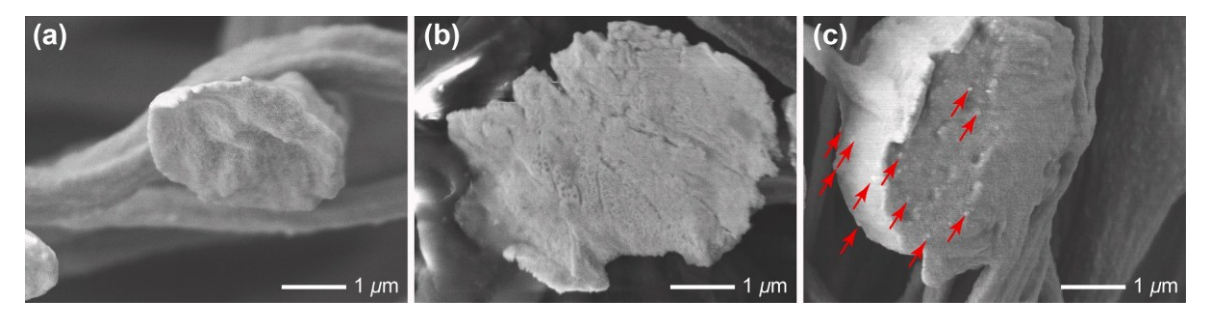


Fig. 5. Cross-section SEM micrographs of nanofibers produced from different electrospinning solutions of (a) NF: PVC [10 wt%, 2000 rpm], (b) NF: PVC-PDMS [10 wt%, 2000 rpm], and (c) NF: PVC-PDMS-ND [10 wt%, 2000 rpm].

S. typhimurium LT2 attachment behavior on electrospun films: influence of preparation conditions.

Attached S. typhimurium LT2 on nanofibers in Log10 CFU/mL

Sample	Concentration	500 rpm	1000 rpm	2000 rpm
PVC	5.0 wt%	6.26 ± 0.41	6.33 ± 0.44	6.04 ± 0.14
	7.5 wt%	6.15 ± 0.15	6.15 ± 0.30	6.29 ± 0.16
	10.0 wt%	5.84 ± 0.37	6.07 ± 0.40	5.94 ± 0.14
PVC-PDMS	5.0 wt%	5.00 ± 0.18	5.22 ± 0.24	5.12 ± 0.18
	7.5 wt%	4.72 ± 0.18	4.56 ± 0.32	4.63 ± 0.33
	10.0 wt%	4.04 ± 0.25	4.26 ± 0.23	4.22 ± 0.07
PVC-PDMS-ND	5.0 wt%	4.63 ± 0.37	4.80 ± 0.27	4.59 ± 0.30
	7.5 wt%	3.37 ± 0.10	3.65 ± 0.19	3.98 ± 0.02
	10.0 wt%	3.57 ± 0.19	3.85 ± 0.26	3.70 ± 0.28

S. typhimurium LT2 on the electrospun thin films under all conditions. The population density of S. typhimurium LT2 on PVC nanofibers ranged from 5.8 to 6.3 Log10 CFU/mL across different concentrations and rotation speeds. Similarly, on PVC/PDMS nanofibers, the range was 4.0 to 5.2 Log10 CFU/mL. Notably, the presence of nanodiamond (ND) significantly reduced bacterial attachment. PVC-PDMS-ND nanofibers, the population density dropped further to 3.4 to 4.8 Log10 CFU/mL. Overall, PVC and PVC-PDMS samples showed higher bacterial attachment compared to PVC-PDMS-ND. This suggests that the addition of ND particles reduces the ability of S. Typhimurium to adhere to the nanofiber surface. Given that the water contact angle (WCA) of fibers containing ND were in the superhydrophobic regime, non-wetting of the aqueous bacterial suspension can explain these observations. In addition, the nanoscale surface roughness introduced by ND protrusions likely minimizes the contact area available for initial bacterial adhesion through the lotus leaf effect (Elbourne et al., 2019; Encinas et al., 2020; Mu et al., 2023). Reduced intimacy of bacterial wall receptors with surface functional groups is detrimental for attachment (Chinnaraj et al., 2021). Furthermore, the faceted ND crystals introduce interfacial surface tension differentials and nanobumps that encourage easier roll-off before bacteria can firmly stick (Arcot et al., 2021; Uzoma et al., 2021; Xu et al., 2020). Superhydrophobic surfaces can also damage cell membrane integrity upon dropping contact lines during wetting state changes. Over longer periods, dynamic motions of sufficiently non-wetting surfaces can also prevent surface conditioning into foul-release states favorable for fouling organisms.

The effect of concentration on bacterial attachment was not straightforward. In pure PVC nanofibers, attachment of S. typhimurium LT2 decreased slightly at higher polymer concentrations, while for PVC-PDMS and PVC-PDMS-ND nanofibers, the trend with respect to concentration was less consistent and did not follow a clear pattern. Drum rotation speed also had a limited impact on bacterial attachment behavior across all nanofiber compositions. No statistically significant differences in attachement were observed across the different rotation speeds within each nanofiber sample group.

Listeria innocua attachment behavior on electrospun films: influence of preparation conditions.

Sample	Concentration	500 rpm	1000 rpm	2000 rpm
PVC	5.0 wt%	5.91 ± 0.44	5.76 ± 0.40	5.75 ± 0.46
	7.5 wt%	5.59 ± 0.21	5.80 ± 0.42	5.61 ± 0.32
	10.0 wt%	5.65 ± 0.14	5.88 ± 0.42	5.75 ± 0.13
PVC-PDMS	5.0 wt%	5.10 ± 0.17	5.13 ± 0.26	5.45 ± 0.25
	7.5 wt%	4.52 ± 0.40	4.60 ± 0.19	4.52 ± 0.25
	10.0 wt%	3.98 ± 0.23	4.53 ± 0.27	4.70 ± 0.21
PVC-PDMS-ND	5.0 wt%	4.19 ± 0.46	4.04 ± 0.21	4.16 ± 0.07
	7.5 wt%	3.40 ± 0.12	3.54 ± 0.10	3.44 ± 0.27
	10.0 wt%	3.24 ± 0.36	3.66 ± 0.20	3.41 ± 0.29

Table 5 highlights the bacteria attachment behavior of *Listeria* (*L*.) innocua on electrospun fibers prepared under different conditions. For pure PVC nanofibers, the L. innocua attachment did not show significant variation across different concentrations and drum rotation speeds. The values hover around 5.6 to 5.9 Log₁₀ CFU/mL, indicating a consistent level of bacterial attachment. The addition of PDMS to PVC resulted in a slight reduction in bacterial attachment. For instance, at a concentration of 5 wt%, the attached L. innocua decreased from around 5.9 Log₁₀ CFU/ mL in pure PVC nanofibers to approximately 5.1 Log₁₀ CFU/mL in PVC-PDMS nanofibers. This reduction became more pronounced at higher concentrations, reaching as low as 3.98 Log₁₀ CFU/mL at 10 wt%. This trend indicates that PDMS imparts some antimicrobial properties to the composite, possibly due to its hydrophobic nature, which might reduce bacterial adhesion. The incorporation of ND into the PVC-PDMS matrix further lowered the bacterial attachment. For example, at 10 wt% concentration, the L. innocua count decreased to around 3.24 Log₁₀ CFU/mL. Similar to S. typhimurium LT2 in Table 4, PVC and PVC-PDMS samples showed higher attachment of L. innocua compared to PVC-PDMS-ND. This reinforces the notion that ND particles reduce bacterial attachment to the nanofibers. Comparing all three materials, it is evident that PVC had the highest bacterial attachment, followed by PVC-PDMS, while PVC-PDMS-ND had the lowest. L. innocua attachment generally exhibited less variation across different concentrations and drum rotation speeds within each sample group compared to S. typhimurium LT2. This could indicate potential differences in the adhesion mechanisms or sensitivity to surface modifications between the two bacterial strains.

The observed differences in L. innocua and S. typhimurium LT2 attachment behavior might be partially attributed to variations in their cell wall structures. S. typhimurium LT2, being a Gram-negative bacterium, has a typical cell wall with an outer membrane, a periplasmic space, and an inner membrane surrounding a thin peptidoglycan layer (Goodell & Higgins, 1987). On the other hand, L. innocua, a Gram-positive bacterium, lacks the outer membrane and possesses a thicker peptidoglycan layer directly surrounding its cytoplasmic membrane (Moorman et al., 2008). Both bacteria express various surface appendages like flagella, fimbriae, and proteins that influence their hydrophobicity and surface charge, ultimately affecting their attachment to surfaces. The slightly lower attachment of L. innocua compared to S. typhimurium LT2 might also be influenced by their different sizes. L. innocua generally has a smaller diameter (0.5–1.0 μ m) and length (0.8-3.0 μm) compared to S. typhimurium LT2, which ranges in diameter from 0.5 to 1.5 μ m and length from 2 to 5 μ m (Liu et al., 2020; Oh et al., 2015; Zhang et al., 2013; Zhou et al., 2024). This size difference could affect their contact area with the nanofibers, potentially contributing to the observed attachment trend.

3.5. Gas permeation behavior of electrospun thin films

Gas permeation testing is crucial for the development and characterization of food packaging materials due to several critical considerations (Zabihzadeh Khajavi et al., 2020; Zare et al., 2022). Adequate barriers to gas transport can help extend food shelf life. Oxygen ingress through packaging causes oxidation, eventually decreasing nutritional content and sensory qualities (Mehyar et al., 2012; Moradinezhad & Dorostkar, 2021). On the other hand, elevated carbon dioxide levels can slow aerobic spoilage by inhibiting microbial growth (Couvert et al., 2023; Yang et al., 2023). However, hermetically blocking all gas diffusion can also be detrimental, leading to the accumulation of metabolites such as carbon dioxide, moisture, or volatile aroma compounds, which adversely affect food quality over time (Groot et al., 2022; Ilhan et al., 2021; D. S. J. Lee et al., 2022). Consequently, a regulated transmission of gases is necessary. Therefore, to understand the permeation behavior of oxygen and carbon dioxide through electrospun thin films, we employed the experimental setup outlined in Fig. S1 in the Supporting Information.

Table 6 summarizes the oxygen permeation trends across all electrospun thin films prepared under varying conditions. PVC samples exhibit the highest oxygen permeation rates compared to PVC-PDMS and PVC-PDMS-ND nanofibers produced across all concentrations and rotation speeds. This suggests that the addition of PDMS and ND into electrospun films reduces oxygen permeation by altering the organization and assembly of the nanofibers. For pure PVC nanofibers, oxygen permeation generally decreases with increasing polymer concentration. This trend could be attributed to increased fiber density and tortuosity of the nanofiber mat at higher concentrations, hindering gas diffusion pathway. However, the effect of concentration on oxygen permeation is less consistent for PVC-PDMS and PVC-PDMS-ND nanofibers. This might be due to the complex interplay between PDMS and ND components, along with variations in fiber morphology, spacing, and orientation at different concentrations. The collector rotation speed exhibits a variable and sometimes inconsistent effect on oxygen permeation across the samples. While some nanofiber compositions show a decrease in permeation at higher speeds, others exhibit the opposite trend or no significant change. This observation suggests that factors beyond just the collector rotation speed, such as fiber alignment, packing density, and interfacial interactions, play a role in governing oxygen transport through these electrospun thin films.

Table 7 summarizes the carbon dioxide permeation trends across all electrospun thin films prepared under varying conditions. For pure PVC nanofibers, a general trend of decreased CO2 permeation with increasing rotation speed was observed, particularly evident at 5 wt% concentration. This trend might indicate tighter packing of fibers into thin films and smaller mesh spacing within the film at higher collector rotation speeds, leading to improved barrier properties. However, the trend was less pronounced at higher concentrations (7.5 wt% and 10 wt%), suggesting that other factors might play a role at elevated concentrations. In PVC-PDMS composite films, the CO₂ permeation showed significant variation based on concentration and rotation speed. Notably, for electrospun films prepared at 5 wt% concentration and 2000 rpm, the permeation was markedly lower (2.20 ± 0.09), indicating superior barrier properties under these conditions. This could be attributed to the enhanced packing and tighter distribution of PDMS-PVC nanofibers, which is faciliated at higher collector rotation speeds. Conversely, at 7.5 wt% and 10 wt% concentrations, the permeation increased, particularly at 1000 rpm and 2000 rpm, suggesting that higher PDMS content might disrupt the fiber packing and mesh spacing, adversely affecting the barrier properties. The inclusion of nanodiamonds in PVC-PDMS nanofibers showed a varied impact on CO2 permeation through the electrospun films. While the permeation values were generally lower than those of pure PVC electrospun film, they did not consistently show

 Table 6

 Oxygen permeation through electrospun films prepared at different conditions.

Gas permeation of Oxygen in cm³/(cm²· s · cmHg) at STP				
Sample	Concentration	500 rpm	1000 rpm	2000 rpm
PVC	5.0 wt%	16.24 ± 3.42	10.99 ± 1.38	4.87 ± 0.56
	7.5 wt%	10.33 ± 1.21	9.35 ± 1.50	7.73 ± 0.95
	10.0 wt%	14.76 ± 1.82	12.90 ± 0.90	11.85 ± 1.49
PVC-PDMS	5.0 wt% 7.5 wt%	4.09 ± 0.10 4.92 ± 0.81	8.10 ± 2.32 13.08 ± 2.11	$2.26 \pm 0.18 3.70 \pm 0.53$
	10.0 wt%	13.87 ± 2.04	14.22 ± 0.90	9.18 ± 1.44
PVC-PDMS-ND	5.0 wt%	10.36 ± 0.70	8.79 ± 0.75	4.85 ± 0.26
	7.5 wt%	12.80 ± 2.28	10.68 ± 1.69	6.22 ± 0.45
	10.0 wt%	13.14 ± 1.97	12.80 ± 1.73	9.82 ± 1.69

Table 7
Carbon dioxide permeation through electrospun thin films prepared at different conditions.

Sample	Concentration	500 rpm	1000 rpm	2000 rpm
PVC	5.0 wt%	19.18 ±	11.23 ±	5.60 ± 0.32
		4.29	3.73	
	7.5 wt%	$12.36 \pm$	$11.81 \pm$	9.77 ± 1.46
		1.05	2.01	
	10.0 wt%	$18.07 \pm$	$15.37 \pm$	11.96 ±
		3.21	2.66	0.59
PVC-PDMS	5.0 wt%	5.35 ± 1.00	8.84 ± 1.46	2.20 ± 0.09
	7.5 wt%	5.52 ± 0.34	$15.25 \pm$	4.97 ± 0.94
			4.02	
	10.0 wt%	$13.68 \pm$	16.1 ± 1.93	8.64 ± 0.35
		1.80		
PVC-PDMS-ND	5.0 wt%	$11.73 \pm$	$10.62 \pm$	6.57 ± 1.71
		1.45	1.78	
	7.5 wt%	$13.43 \pm$	$10.03 \pm$	8.15 ± 0.49
		2.15	0.74	
	10.0 wt%	$13.52 \pm$	$11.52 \pm$	9.62 ± 1.25
		1.52	1.42	

improvement over electrospun PVC-PDMS composite films. This observation implies that while ND contributes to the barrier properties, their effectiveness might be dependent on the interplay between concentration, processing conditions, and the resulting fiber morphology and packing.

4. Conclusion

In summary, this work describes a versatile, single-step method to generate bacterially antifouling food packaging films via electrospinning composites of polyvinyl chloride (PVC), polydimethylsiloxane (PDMS), and nanodiamond (ND) onto a rotating drum collector. It was found that varying the PVC, PDMS, and ND concentrations along with drum rotational speed modulated the ultimate fiber diameters from 0.4 to 2.0 µm. Such variations also allowed tuning of water contact angles spanning 136.2-159.5° on resultant electrospun surfaces. Pure PVC based films displayed the most hydrophilic wetting response while materials fabricated with PVC-PDMS-ND blends achieved superhydrophobic enhancement up to ~160°. Matching this boosted water repellency, nanocomposites with ND and PVC-PDMS mixtures significantly reduced adhesion against Salmonella typhimurium LT2 and Listeria innocua cultures, realizing ~99.6-99.8 % bacterial density reductions versus analogous pure PVC-only films. Tensile strength was elevated from 1.2 MPa for pristine polymeric PVC samples up to 8.9 MPa for optimized PVC-PDMS-ND blends. By modulating electrospinning parameters across all samples and processing conditions, the upper limit for oxygen permeation of 19.2 cm³/(cm² · s · cmHg) at STP could be achieved, while the lower limit was around 2.2 cm³/(cm² · s · cmHg) at STP. Similarly, the upper limit for carbon dioxide permeation was around 18.1 cm 3 /(cm $^2 \cdot s \cdot cmHg$) at STP, with the lower limit being approximately 2.2 cm³/(cm² · s · cmHg) at STP. Overall, via interfacially tailored compositions and emergent morphological responses from tunable single-step electrospinning, these active films advance ecofriendly food storage solutions, resisting microbial hazards by synergistically integrating critical functional traits like biofouling mitigation, physical durability, and nanotechnology-enabled performance enhancements, paving the way toward a safer and healthier food supply chain.

Ethical statement

The authors declare that the research presented does not involve any animal or human study.

CRediT authorship contribution statement

Shuhao Liu: Writing – original draft, Resources, Methodology, Investigation, Conceptualization. Monica Iepure: Writing – review & editing, Validation, Formal analysis. Wentao Zhou: Writing – review & editing, Methodology, Investigation. William DeFlorio: Methodology, Investigation. Mustafa E.S. Akbulut: Writing – review & editing, Supervision, Funding acquisition, Conceptualization. Younjin Min: Writing – review & editing, Visualization, Funding acquisition, Conceptualization, Validation, Formal analysis.

Declaration of competing interest

The authors declare that they have no known competing financial interests or personal relationships that could have appeared to influence the work reported in this paper.

Data availability

Data will be made available on request.

Acknowledgements

The authors acknowledge that some of the characterization part of this work was performed at the Texas A&M University Materials Characterization Core Facility. Use of the Texas A&M University Soft Matter Facility and the contributions of Dr. Wei are acknowledged. This work was partially supported by the Food Manufacturing Technologies Program A1363 (Grant Number 2019–68015–29231, Project Number TEX09762) from the United States Department of Agriculture (USDA). This work was also partly supported by the USDA National Institute of Food and Agriculture - Specialty Crop Research Initiative (SCRI) under the C-REEMS Grant Number 2021–07786 and the tracking number GRANT13369273, as well as the National Science Foundation - Chemical, Bioengineering, Environmental and Transport Systems under Grant Number 2040301, and Civil, Mechanical and Manufacturing Innovation under Grant Number 1826250.

Supplementary materials

Supplementary material associated with this article can be found, in the online version, at doi:10.1016/j.afres.2024.100417.

References

- Ait-Touchente, Z., Khellaf, M., Raffin, G., Lebaz, N., & Elaissari, A. (2023). Recent advances in polyvinyl chloride (PVC) recycling. *Polymers for Advanced Technologies*, e6228.
- Alamri, M. S., Qasem, A. A. A., Mohamed, A. A., Hussain, S., Ibraheem, M. A., Shamlan, G., Alqah, H. A., & Qasha, A. S. (2021). Food packaging's materials: A food safety perspective. Saudi Journal of Biological Sciences, 28(8), 4490–4499. https:// doi.org/10.1016/j.sjbs.2021.04.047
- Arcot, Y., Liu, S., Ulugun, B., DeFlorio, W., Bae, M., Salazar, K. S., Taylor, T. M., Castillo, A., Cisneros-Zevallos, L., & Scholar, E. M. (2021). Fabrication of robust superhydrophobic coatings onto high-density polyethylene food contact surfaces for enhanced microbiological food safety. ACS Food Science & Technology, 1(7), 1180–1189.
- Arcot, Y., Mu, M., Taylor, T. M., Castillo, A., Cisneros-Zevallos, L., & Akbulut, M. E. (2023). Essential Oil Vapors Assisted Plasma for Rapid, Enhanced Sanitization of Food-Associated Pathogenic Bacteria. Food and Bioprocess Technology, 1–18.
- Arora, A., & Padua, G. (2010). Nanocomposites in food packaging. *Journal of Food science*, 75(1), R43–R49.
- Asghari, M., Sheikh, M., & Dehghani, M. (2018). Comparison of ZnO nanofillers of different shapes on physical, thermal and gas transport properties of PEBA membrane: experimental testing and molecular simulation. *Journal of Chemical Technology & Biotechnology*, 93(9), 2602–2616.
- Ballesteros, V., Costa, O., Iniguez, C., Fletcher, T., Ballester, F., & Lopez-Espinosa, M.-J. (2017). Exposure to perfluoroalkyl substances and thyroid function in pregnant women and children: a systematic review of epidemiologic studies. *Environment* international, 99, 15–28.

- Bangar, S. P., Whiteside, W. S., Ashogbon, A. O., & Kumar, M. (2021). Recent advances in thermoplastic starches for food packaging: A review. Food Packaging and Shelf Life, 30 Article 100743
- Barbosa, J., Albano, H., Silva, C., & Teixeira, P. (2019). Microbiological contamination of reusable plastic bags for food transportation. Food Control, 99, 158–163.
- Bormashenko, E. (2019). Apparent contact angles for reactive wetting of smooth, rough, and heterogeneous surfaces calculated from the variational principles. *Journal of Colloid and Interface Science*, 537, 597–603.
- Camerlo, A., Vebert-Nardin, C., Rossi, R. M., & Popa, A. M. (2013). Fragrance encapsulation in polymeric matrices by emulsion electrospinning. *European Polymer Journal*, 49(12), 3806–3813. https://doi.org/10.1016/j.eurpolymj.2013.08.028
- Caron-Beaudoin, E´., Ayotte, P., Sidi, E. A. L., of Nutashkuan, C. T. K., McHugh, N. G.-L., & Lemire, M. (2019). Exposure to perfluoroalkyl substances (PFAS) and associations with thyroid parameters in First Nation children and youth from Quebec. *Environment international*, 128, 13–23.
- Castro Coelho, S., Nogueiro Estevinho, B., & Rocha, F. (2021). Encapsulation in food industry with emerging electrohydrodynamic techniques: Electrospinning and electrospraying – A review. Food Chemistry, 339, Article 127850. https://doi.org/ 10.1016/j.foodchem.2020.127850
- Chauhan, S., Jain, N., & Nagaich, U. (2020). Nanodiamonds with powerful ability for drug delivery and biomedical applications: Recent updates on in vivo study and patents. *Journal of pharmaceutical analysis*, 10(1), 1–12.
- Chavoshnejad, P., & Razavi, M. J. (2020). Effect of the interfiber bonding on the mechanical behavior of electrospun fibrous mats. *Scientific Reports*, 10(1), 7709.
- Chen, S., Brahma, S., Mackay, J., Cao, C., & Aliakbarian, B. (2020). The role of smart packaging system in food supply chain. *Journal of Food Science*, 85(3), 517–525. https://doi.org/10.1111/1750-3841.15046
- Chinnaraj, S. B., Jayathilake, P. G., Dawson, J., Ammar, Y., Portoles, J., Jakubovics, N., & Chen, J. (2021). Modelling the combined effect of surface roughness and topography on bacterial attachment. *Journal of Materials Science & Technology*, 81, 151–161.
- Costa, S. M., Ferreira, D. P., Teixeira, P., Ballesteros, L. F., Teixeira, J. A., & Fangueiro, R. (2021). Active natural-based films for food packaging applications: The combined effect of chitosan and nanocellulose. *International Journal of Biological Macromolecules*, 177, 241–251.
- Couvert, O., Koullen, L., Lochardet, A., Huchet, V., Thevenot, J., & Le Marc, Y (2023). Effects of carbon dioxide and oxygen on the growth rate of various food spoilage bacteria. Food Microbiology, 114, Article 104289.
- Cremaldi, J., & Bhushan, B. (2018). Fabrication of bioinspired, self-cleaning superliquiphilic/phobic stainless steel using different pathways. *Journal of Colloid* and Interface Science, 518, 284–297.
- da Silva, R. G., Malta, M. I., de Carvalho, L. A., da Silva, J. J., da Silva Filho, W. L., Oliveira, S. H., de Araújo, E. G., Urtiga Filho, S. L., & Vieira, M. R. (2023). Low-cost superhydrophobic coating on aluminum alloy with self-cleaning and repellency to water-based mixed liquids for anti-corrosive applications. Surface and Coatings Technology, 457, Article 129293.
- De Feudis, M., Tallaire, A., Nicolas, L., Brinza, O., Goldner, P., He´tet, G., B´en´edic, F., & Achard, J. (2020). Large-scale fabrication of highly emissive nanodiamonds by chemical vapor deposition with controlled doping by SiV and GeV centers from a solid source. *Advanced Materials Interfaces*, 7(2), Article 1901408.
- DeFlorio, W., Liu, S., White, A. R., Taylor, T. M., Cisneros-Zevallos, L., Min, Y., & Scholar, E. M. A. (2021). Recent developments in antimicrobial and antifouling coatings to reduce or prevent contamination and cross-contamination of food contact surfaces by bacteria. Comprehensive Reviews in Food Science and Food Safety, 20(3), 3093–3134. https://doi.org/10.1111/1541-4337.12750
- Di Ciccio, P., Rubiola, S., Grassi, M. A., Civera, T., Abbate, F., & Chiesa, F. (2020). Fate of Listeria monocytogenes in the presence of resident cheese microbiota on common packaging materials. Frontiers in Microbiology, 11, 830.
- Dickman, R. A., & Aga, D. S. (2022). A review of recent studies on toxicity, sequestration, and degradation of per-and polyfluoroalkyl substances (PFAS). *Journal of Hazardous Materials*, 436, Article 129120.
- Elbourne, A., Chapman, J., Gelmi, A., Cozzolino, D., Crawford, R. J., & Truong, V. K. (2019). Bacterial-nanostructure interactions: The role of cell elasticity and adhesion forces. *Journal of Colloid and Interface Science*, 546, 192–210.
- Encinas, N., Yang, C.-Y., Geyer, F., Kaltbeitzel, A., Baumli, P., Reinholz, J., Mail "ander, V., Butt, H.-J.r., & Vollmer, D. (2020). Submicrometer-sized roughness suppresses bacteria adhesion. ACS applied materials & interfaces, 12(19), 21192–21200.
- Erbil, H. Y. (1994). Calculation of spreading pressure from contact angle data on polymer surfaces. *Langmuir*, 10(6), 2006–2009.
- Faccini, M., Vaquero, C., & Amantia, D. (2012). Development of Protective Clothing against Nanoparticle Based on Electrospun Nanofibers. *Journal of Nanomaterials*, 2012, Article 892894. https://doi.org/10.1155/2012/892894
- Facts, P. (2019). An analysis of European plastics production, demand and waste data. Plastics Europe.
- Fernandez, A., Torres-Giner, S., & Lagaron, J. M. (2009). Novel route to stabilization of bioactive antioxidants by encapsulation in electrospun fibers of zein prolamine. Food Hydrocolloids, 23(5), 1427–1432. https://doi.org/10.1016/j.foodhyd.2008.10.011
- Giannakourou, M. C., & Tsironi, T. N. (2021). Application of Processing and Packaging Hurdles for Fresh-Cut Fruits and Vegetables Preservation. Foods, 10(4), 830. https://www.mdpi.com/2304-8158/10/4/830.
- Goodell, E. W., & Higgins, C. F. (1987). Uptake of cell wall peptides by Salmonella typhimurium and Escherichia coli. *Journal of bacteriology*, 169(8), 3861–3865.
- Groot, S. P., Van Litsenburg, M.-J., Kodde, J., Hall, R. D., de Vos, R. C., & Mumm, R. (2022). Analyses of metabolic activity in peanuts under hermetic storage at different relative humidity levels. *Food Chemistry*, 373, Article 131020.
- Hamid, N., Junaid, M., Manzoor, R., Sultan, M., Chuan, O. M., & Wang, J. (2023). An integrated assessment of ecological and human health risks of per-and

- polyfluoroalkyl substances through toxicity prediction approaches. *Science of The Total Environment*, Article 167213.
- Hammons, J. A., Nielsen, M. H., Bagge-Hansen, M., Bastea, S., May, C., Shaw, W. L., Martin, A., Li, Y., Sinclair, N., & Lauderbach, L. M. (2021). Submicrosecond aggregation during detonation synthesis of nanodiamond. *The Journal of Physical Chemistry Letters*, 12(22), 5286–5293.
- Han, J.-W., Ruiz-Garcia, L., Qian, J.-P., & Yang, X.-T. (2018). Food Packaging: A Comprehensive Review and Future Trends. Comprehensive Reviews in Food Science and Food Safety, 17(4), 860–877. https://doi.org/10.1111/1541-4337.12343
- Hashemi, H., Hashemi, M., Talcott, S., Castillo, A., Taylor, T. M., & Akbulut, M. (2022). Nanoimbibition of Essential Oils in Triblock Copolymeric Micelles as Effective Nanosanitizers against Food Pathogens Listeria monocytogenes and Escherichia coli O157: H7. ACS Food Science & Technology, 2(2), 290–301.
- Holmquist, H., Fantke, P., Cousins, I. T., Owsianiak, M., Liagkouridis, I., & Peters, G. M. (2020). An (eco) toxicity life cycle impact assessment framework for per-and polyfluoroalkyl substances. *Environmental science & technology*, 54(10), 6224–6234.
- Hong, P.-D., & Chen, J.-H. (1999). Molecular aggregation behaviour of poly (vinyl chloride) solutions. *Polymer*, 40(14), 4077–4085.
- Huang, J., Cai, Y., Xue, C., Ge, J., Zhao, H., & Yu, S.-H. (2021). Highly stretchable, soft and sticky PDMS elastomer by solvothermal polymerization process. *Nano Research*, 14, 3636–3642.
- Ilhan, I., Turan, D., Gibson, I., & ten Klooster, R. (2021). Understanding the factors affecting the seal integrity in heat sealed flexible food packages: A review. *Packaging technology and science*, 34(6), 321–337.
- Iqbal, S., Rafique, M. S., Zahid, M., Bashir, S., Ahmad, M. A., & Ahmad, R. (2018). Impact of carrier gas flow rate on the synthesis of nanodiamonds via microplasma technique. *Materials Science in Semiconductor Processing*, 74, 31-41.
- Khedkar, D., & Khedkar, R (2020). New Innovations in Food Packaging in Food Industry. In M. Thakur, & V. K. Modi (Eds.), Emerging Technologies in Food Science: Focus on the Developing World (pp. 165-185). Singapore: Springer. https://doi.org/10.1007/978-981-15-2556-8 15.
- Kirchner, M., Goulter, R. M., Chapman, B. J., Clayton, J., & Jaykus, L.-A. (2021). Cross-contamination on atypical surfaces and venues in food service environments. *Journal of food protection*, 84(7), 1239–1251.
- Konstantoglou, A., Folinas, D., & Fotiadis, T. (2020). Exploring the Multi-Function Nature of Packaging in the Food Industry. *Logistics*, 4(3), 21. https://www.mdpi.com/2305.65904(3)21
- Kumar, S., Nehra, M., Kedia, D., Dilbaghi, N., Tankeshwar, K., & Kim, K.-H. (2019).Nanodiamonds: Emerging face of future nanotechnology. Carbon, 143, 678–699.
- Lamberti, A., Quaglio, M., Sacco, A., Cocuzza, M., & Pirri, C. (2012). Surface energy tailoring of glass by contact printed PDMS. Applied Surface Science, 258(23), 0477-0421
- Lebar, A., Aguiar, R., Oddy, A., & Petel, O. E. (2021). Particle surface effects on the spall strength of particle-reinforced polymer matrix composites. *International Journal of Impact Engineering*, 150, Article 103801.
- Lee, J., Seo, J., Cho, K. M., Heo, J., Jung, H., Park, S., Bae, J., Lee, S., Hong, J., & Kim, M.-K. (2022). Ultralight and Ultrathin Electrospun Membranes with Enhanced Air Permeability for Chemical and Biological Protection. ACS applied materials & interfaces, 14(28), 32522–32532.
- Li, S., Liu, Y., Zheng, Z., Liu, X., Huang, H., Han, Z., & Ren, L. (2019). Biomimetic robust superhydrophobic stainless-steel surfaces with antimicrobial activity and molecular dynamics simulation. *Chemical Engineering Journal*, 372, 852–861.
- Liu, C., Hsu, P.-C., Lee, H.-W., Ye, M., Zheng, G., Liu, N., Li, W., & Cui, Y. (2015). Transparent air filter for high-efficiency PM2.5 capture. *Nature Communications*, 6 (1), 6205. https://doi.org/10.1038/ncomms7205
- Liu, S., Ulugun, B., DeFlorio, W., Arcot, Y., Yegin, Y., Salazar, K. S., Castillo, A., Taylor, T. M., Cisneros-Zevallos, L., & Akbulut, M. (2021). Development of durable and superhydrophobic nanodiamond coating on aluminum surfaces for improved hygiene of food contact surfaces. *Journal of Food Engineering*, 298, Article 110487.
- Liu, S., Zheng, J., Hao, L., Yegin, Y., Bae, M., Ulugun, B., Taylor, T. M., Scholar, E. A., Cisneros-Zevallos, L., & Oh, J. K. (2020). Dual-functional, superhydrophobic coatings with bacterial anticontact and antimicrobial characteristics. ACS applied materials & interfaces, 12(19), 21311–21321.
- Liu, Y., Sameen, D. E., Ahmed, S., Dai, J., & Qin, W. (2021). Antimicrobial peptides and their application in food packaging. *Trends in Food Science & Technology*, 112, 471–483.
- Lo´pez-Ga´Ivez, F., Rasines, L., Conesa, E., Go´mez, P. A., Art´es-Herna´ndez, F., & Aguayo, E. (2021). Reusable Plastic Crates (RPCs) for Fresh Produce (Case Study on Cauliflowers): Sustainable Packaging but Potential Salmonella Survival and Risk of Cross-Contamination. Foods, 10(6), 1254. https://www.mdpi.com/2304-8158/10/6/1254.
- Lo "ßlein, S. M., Mücklich, F., & Grützmacher, P. G. (2022). Topography versus chemistry-How can we control surface wetting? *Journal of Colloid and Interface Science*, 609, 645-656.
- Luber, P., Brynestad, S., Topsch, D., Scherer, K., & Bartelt, E. (2006). Quantification of Campylobacter species cross-contamination during handling of contaminated fresh chicken parts in kitchens. Applied and environmental microbiology, 72(1), 66–70.
- Marsh, K., & Bugusu, B. (2007). Food packaging—roles, materials, and environmental issues. *Journal of food science*, 72(3), R39–R55.
- Mehyar, G. F., Al-Ismail, K., Han, J. H., & Chee, G. W. (2012). Characterization of edible coatings consisting of pea starch, whey protein isolate, and carnauba wax and their effects on oil rancidity and sensory properties of walnuts and pine nuts. *Journal of Food science*, 77(2), E52–E59.
- Mohammadalinejhad, S., Almasi, H., & Esmaiili, M. (2021). Physical and release properties of poly(lactic acid)/nanosilver-decorated cellulose, chitosan and

- lignocellulose nanofiber composite films. *Materials Chemistry and Physics*, 268, Article 124719. https://doi.org/10.1016/j.matchemphys.2021.124719
- Mohammadzadeh-Vazifeh, M. M., Hosseini, S. M., Khajeh-Nasiri, S., Hashemi, S., & Fakhari, J. (2015). Isolation and identification of bacteria from paperboard food packaging. *Iranian Journal of Microbiology*, 7(5), 287.
- Mohsin, A., Zaman, W. Q., Guo, M., Ahmed, W., Khan, I. M., Niazi, S., Rehman, A., Hang, H., & Zhuang, Y. (2020). Xanthan-Curdlan nexus for synthesizing edible food packaging films. *International Journal of Biological Macromolecules*, 162, 43–49.
- Moorman, M. A., Thelemann, C. A., Zhou, S., Pestka, J. J., Linz, J. E., & Ryser, E. T. (2008). Altered hydrophobicity and membrane composition in stress-adapted Listeria innocua. *Journal of food protection*, 71(1), 182–185.
- Moradinezhad, F., & Dorostkar, M. (2021). Effect of vacuum and modified atmosphere packaging on the quality attributes and sensory evaluation of fresh jujube fruit. *International Journal of Fruit Science*, 21(1), 82-94.
- Mu, M., Liu, S., DeFlorio, W., Hao, L., Wang, X., Salazar, K. S., Taylor, M., Castillo, A., Cisneros-Zevallos, L., & Oh, J. K. (2023). Influence of Surface Roughness, Nanostructure, and Wetting on Bacterial Adhesion. *Langmuir*, 39(15), 5426–5439.
- Mu, M., Wang, X., Taylor, M., Castillo, A., Cisneros-Zevallos, L., Akbulut, M., & Min, Y. (2023). Multifunctional coatings for mitigating bacterial fouling and contamination. Colloid and Interface Science Communications, 55, Article 100717.
- Nethra, P. V., Sunooj, K. V., Aaliya, B., Navaf, M., Akhila, P. P., Sudheesh, C., Mir, S. A., Shijin, A., & George, J. (2023). Critical factors affecting the shelf life of packaged fresh red meat – A review. *Measurement: Food, 10*, Article 100086. https://doi.org/ 10.1016/j.meafoo.2023.100086
- Newsome, R., Balestrini, C. G., Baum, M. D., Corby, J., Fisher, W., Goodburn, K., Labuza, T. P., Prince, G., Thesmar, H. S., & Yiannas, F. (2014). Applications and perceptions of date labeling of food. *Comprehensive Reviews in Food Science and Food Safety*, 13(4), 745–769.
- Oh, J., Schmidt, R. J., Tancredi, D., Calafat, A. M., Roa, D. L., Hertz-Picciotto, I., & Shin, H.-M. (2021). Prenatal exposure to per-and polyfluoroalkyl substances and cognitive development in infancy and toddlerhood. *Environmental research*, 196, Article 110939.
- Oh, J. K., Liu, S., Jones, M., Yegin, Y., Hao, L., Tolen, T. N., Nagabandi, N., Scholar, E. A., Castillo, A., & Taylor, T. M. (2019). Modification of aluminum surfaces with superhydrophobic nanotextures for enhanced food safety and hygiene. Food Control, 96, 463–469.
- Oh, J. K., Perez, K., Kohli, N., Kara, V., Li, J., Min, Y., Castillo, A., Taylor, M., Jayaraman, A., & Cisneros-Zevallos, L. (2015). Hydrophobically-modified silica aerogels: Novel food-contact surfaces with bacterial anti-adhesion properties. Food Control, 52, 132–141.
- Omer, S., Forga´ch, L., Zelko´, R., & Sebe, I. (2021). Scale-up of Electrospinning: Market Overview of Products and Devices for Pharmaceutical and Biomedical Purposes. *Pharmaceutics*, 13(2), 286. https://www.mdpi.com/1999-4923/13/2/286.
- Patrignani, F., Siroli, L., Gardini, F., & Lanciotti, R. (2016). Contribution of Two Different Packaging Material to Microbial Contamination of Peaches: Implications in Their Microbiological Quality [Original Research]. Frontiers in Microbiology, 7. https://doi. org/10.3389/fmicb.2016.00938
- Rammak, T., Boonsuk, P., & Kaewtatip, K. (2021). Mechanical and barrier properties of starch blend films enhanced with kaolin for application in food packaging. *International Journal of Biological Macromolecules*, 192, 1013–1020.
- Rashid, T. U., Gorga, R. E., & Krause, W. E. (2021). Mechanical properties of electrospun fibers—a critical review. Advanced Engineering Materials, 23(9), Article 2100153.
- Rejeesh, C. R., & Anto, T. (2023). Packaging of milk and dairy products: Approaches to sustainable packaging. *Materials Today: Proceedings*, 72, 2946–2951. https://doi.org/ 10.1016/j.matpr.2022.07.467
- Schaider, L. A., Balan, S. A., Blum, A., Andrews, D. Q., Strynar, M. J., Dickinson, M. E., Lunderberg, D. M., Lang, J. R., & Peaslee, G. F. (2017). Fluorinated compounds in US fast food packaging. Environmental science & technology letters, 4(3), 105-111.
- Sharma, S., Jaiswal, S., Duffy, B., & Jaiswal, A. K. (2022). Advances in emerging technologies for the decontamination of the food contact surfaces. *Food Research International*, 151, Article 110865.
- Shenoy, S. L., Bates, W. D., & Wnek, G. (2005). Correlations between electrospinnability and physical gelation. *Polymer*, 46(21), 8990–9004.
- Siroli, L., Patrignani, F., Serrazanetti, D. I., Chiavari, C., Benevelli, M., Grazia, L., & Lanciotti, R. (2017). Survival of spoilage and pathogenic microorganisms on cardboard and plastic packaging materials. Frontiers in Microbiology, 8, 2606.
- Spence, C. (2016). Multisensory packaging design: Color, shape, texture, sound, and smell. Integrating the packaging and product experience in food and beverages, 1–22.
- Steenland, K., & Winquist, A. (2021). PFAS and cancer, a scoping review of the epidemiologic evidence. Environmental research, 194, Article 110690.
- Sun, C., McClure, J., Berg, S., Mostaghimi, P., & Armstrong, R. T. (2022). Universal description of wetting on multiscale surfaces using integral geometry. *Journal of Colloid and Interface Science*, 608, 2330–2338.
- Sun, Y., Zhao, X., Xu, X., Ma, Y., Guan, H., Liang, H., & Wang, D. (2021). Monitoring of transfer and internalization of Escherichia coli from inoculated knives to fresh cut cucumbers (Cucumis sativus L.) using bioluminescence imaging. Scientific Reports, 11 (1), 11425.
- Sydow, Z., & Bien´czak, K. (2019). The overview on the use of natural fibers reinforced composites for food packaging. *Journal of Natural Fibers*, 16(8), 1189–1200. https://doi.org/10.1080/15440478.2018.1455621
- Tan, S. M., Teoh, X. Y., Le Hwang, J., Khong, Z. P., Sejare, R., Almashhadani, A. Q., Assi, R. A., & Chan, S. Y (2022). Electrospinning and its potential in fabricating pharmaceutical dosage form. *Journal of Drug Delivery Science and Technology*, 76, Article 103761. https://doi.org/10.1016/j.jddst.2022.103761
- Torres Dominguez, E., Nguyen, P. H., Hunt, H. K., & Mustapha, A. (2019). Antimicrobial coatings for food contact surfaces: Legal framework, mechanical properties, and

- potential applications. Comprehensive Reviews in Food Science and Food Safety, 18(6), 1825–1858.
- Uzoma, P. C., Wang, Q., Zhang, W., Gao, N., Li, J., Okonkwo, P. C., Liu, F., & Han, E.-H. (2021). Anti-bacterial, icephobic, and corrosion protection potentials of superhydrophobic nanodiamond composite coating. *Colloids and Surfaces A: Physicochemical and Engineering Aspects*, 630, Article 127532.
- Vasile, C., & Baican, M. (2021). Progresses in Food Packaging, Food Quality, and Safety—Controlled-Release Antioxidant and/or Antimicrobial Packaging. *Molecules*, 26(5), 1263. https://www.mdpi.com/1420-3049/26/5/1263.
- Vass, P., Szabo´, E., Domokos, A., Hirsch, E., Galata, D., Farkas, B., De´muth, B., Andersen, S. K., Vigh, T., Verreck, G., Marosi, G., & Nagy, Z. K. (2020). Scale-up of electrospinning technology: Applications in the pharmaceutical industry. WIREs Nanomedicine and Nanobiotechnology, 12(4), e1611. https://doi.org/10.1002/ wpan.1611
- Vega-Lugo, A.-C., & Lim, L.-T. (2009). Controlled release of allyl isothiocyanate using soy protein and poly(lactic acid) electrospun fibers. Food Research International, 42(8), 933–940. https://doi.org/10.1016/j.foodres.2009.05.005
- Wang, G., Li, A., Li, K., Zhao, Y., Ma, Y., & He, Q. (2021). A fluorine-free superhydrophobic silicone rubber surface has excellent self-cleaning and bouncing properties. *Journal of Colloid and Interface Science*, 588, 175–183.
- Wen, P., Zhu, D.-H., Wu, H., Zong, M.-H., Jing, Y.-R., & Han, S.-Y. (2016). Encapsulation of cinnamon essential oil in electrospun nanofibrous film for active food packaging. Food Control, 59, 366–376. https://doi.org/10.1016/j.foodcont.2015.06.005
- Wen, S, Hu, Y, Zhang, Y, Huang, S, Zuo, Y, & Min, Y (2019). Dual-functional core-shell electrospun mats with precisely controlled release of anti-inflammatory and antibacterial agents. *Materials Science and Engineering: C, 100*, 514–522.
- Wool, R. P. (1993). Polymer entanglements. Macromolecules, 26(7), 1564-1569.
- Xing, L., Liu, C., Zhang, Q., Yu, J., Gong, X., Yu, D., Dai, C., & Feng, Y. (2023). Synergistic effect of micro-and nano-structure for superhydrophobic surfaces. *Materials Today Communications*, 34, Article 105229.
- Xu, L., Zhao, Q., Li, Y., He, F., Zhou, Y., He, R., Fan, J., Zhang, K., & Yang, W. (2020). Nanodiamond-modified microencapsulated phase-change materials with superhydrophobicity and high light-to-thermal conversion efficiency. *Industrial & Engineering Chemistry Research*, 59(50), 21736–21744.
- Xu, Q., Pang, M., Zhu, L., Zhang, Y., & Feng, S. (2010). Mechanical properties of silicone rubber composed of diverse vinyl content silicone gums blending. *Materials & Design*, 31(9) 4083–4087
- Xu, S., Wang, Q., & Wang, N. (2021). Chemical fabrication strategies for achieving bioinspired superhydrophobic surfaces with micro and nanostructures: a review. *Advanced Engineering Materials*, 23(3), Article 2001083.
- Xue, J., Wu, T., Dai, Y., & Xia, Y. (2019). Electrospinning and electrospun nanofibers: Methods, materials, and applications. Chemical reviews, 119(8), 5298-5415.
- Yang, J., Liang, R., Mao, Y., Dong, P., Zhu, L., Luo, X., Zhang, Y., & Yang, X. (2023). Potential inhibitory effect of carbon dioxide on the spoilage behaviors of Pseudomonas fragi in high-oxygen packaged beef during refrigerated storage. Food Microbiology, 112, Article 104229.
- Yang, K., Shi, J., Wang, L., Chen, Y., Liang, C., Yang, L., & Wang, L.-N. (2022). Bacterial anti-adhesion surface design: Surface patterning, roughness and wettability: A review. *Journal of Materials Science & Technology*, 99, 82–100.
- Yilbas, B. S., Hassan, G., Al-Qahtani, H., Al-Sharafi, A., & Sahin, A. (2021). Dust mitigation by rolling water droplets from hydrophobic surfaces. *Surfaces and Interfaces*, 22, Article 100825.
- Yu, C., Sasic, S., Liu, K., Salameh, S., Ras, R. H., & van Ommen, J. R. (2020).
 Nature-Inspired self-cleaning surfaces: Mechanisms, modelling, and manufacturing.
 Chemical Engineering Research and Design, 155, 48-65.

- Yuan, Y., Peng, C., Sun, T., Chen, D., Gao, C., Li, S., & Wu, Z. (2021). Influences of particle content, size and particle/matrix bonding strength on the gas transmission coefficient of carbon fiber reinforced epoxy. *Composites Science and Technology*, 216, Article 109071.
- Zabihzadeh Khajavi, M., Ebrahimi, A., Yousefi, M., Ahmadi, S., Farhoodi, M., Mirza Alizadeh, A., & Taslikh, M. (2020). Strategies for producing improved oxygen barrier materials appropriate for the food packaging sector. Food Engineering Reviews, 12, 346– 363.
- Zaman, Q., Zia, K. M., Zuber, M., Mabkhot, Y. N., Almalki, F., & Hadda, T. B. (2019). A comprehensive review on synthesis, characterization, and applications of polydimethylsiloxane and copolymers. *International Journal of Plastics Technology*, 23, 261-282.
- Zare, M., Namratha, K., Ilyas, S., Sultana, A., Hezam, A., Surmeneva, M. A., Surmenev, R. A., Nayan, M., Ramakrishna, S., & Mathur, S. (2022). Emerging trends for ZnO nanoparticles and their applications in food packaging. ACS Food Science & Technology, 2(5), 763-781.
- Zhang, C., Li, Y., Wang, P., & Zhang, H. (2020). Electrospinning of nanofibers: Potentials and perspectives for active food packaging. Comprehensive Reviews in Food Science and Food Safety, 19(2), 479–502. https://doi.org/10.1111/1541-4337.12536
- Zhang, F., Si, Y., Yu, J., & Ding, B. (2023). Electrospun porous engineered nanofiber materials: A versatile medium for energy and environmental applications. *Chemical Engineering Journal*, 456, Article 140989.
- Zhang, M., Oh, J. K., Cisneros-Zevallos, L., & Akbulut, M. (2013). Bactericidal effects of nonthermal low-pressure oxygen plasma on S. typhimurium LT2 attached to fresh produce surfaces. *Journal of Food Engineering*, 119(3), 425–432.
- Zhang, M., Oh, J. K., Huang, S.-Y., Lin, Y.-R., Liu, Y., Mannan, M. S., Cisneros-Zevallos, L., & Akbulut, M. (2015). Priming with nano-aerosolized water and sequential dip-washing with hydrogen peroxide: An efficient sanitization method to inactivate Salmonella Typhimurium LT2 on spinach. *Journal of Food Engineering*, 161, 8–15.
- Zhang, M., Yang, F., Pasupuleti, S., Oh, J. K., Kohli, N., Lee, I.-S., Perez, K., Verkhoturov, S. V., Schweikert, E. A., & Jayaraman, A. (2014). Preventing adhesion of Escherichia coli O157: H7 and Salmonella Typhimurium LT2 on tomato surfaces via ultrathin polyethylene glycol film. *International journal of food microbiology*, 185, 73-81
- Zhang, Y., Wang, T., Wu, M., & Wei, W. (2021). Durable superhydrophobic surface with hierarchical microstructures for efficient water collection. Surface and Coatings Technology, 419, Article 127279.
- Zhao, L., Duan, G., Zhang, G., Yang, H., He, S., & Jiang, S. (2020). Electrospun Functional Materials toward Food Packaging Applications: A Review. *Nanomaterials*, 10(1), 150. https://www.mdpi.com/2079-4991/10/1/150.
- Zhou, W., Liu, S., DeFlorio, W., Song, S. H., Choi, H., Cisneros-Zevallos, L., Oh, J. K., & Akbulut, M. E. (2024). Nanostructured antifouling coatings for galvanized steel food storage and container surfaces to enhance hygiene and corrosion resistance against bacterial, fungal, and mud contamination. *Journal of Food Engineering*, 363, Article 111784.
- Zhu, Z., Zhang, Y., Shang, Y., & Wen, Y. (2019). Electrospun Nanofibers Containing TiO2 for the Photocatalytic Degradation of Ethylene and Delaying Postharvest Ripening of Bananas. Food and Bioprocess Technology, 12(2), 281–287. https://doi.org/10.1007/ s11947-018-2207-1
- Zouaghi, S., Six, T., Bellayer, S., Moradi, S., Hatzikiriakos, S. G., Dargent, T., Thomy, V., Coffinier, Y., Andr´e, C., & Delaplace, G. (2017). Antifouling biomimetic liquidinfused stainless steel: application to dairy industrial processing. ACS applied materials & interfaces, 9(31), 26565–26573.